The effect of loading rate on static friction and the rate of fault healing during the earthquake cycle

Chris Marone

Department of Earth, Atmospheric, and Planetary Sciences, MIT, Cambridge, Massachusetts 02139, USA

The seismic cycle requires that faults strengthen (heal) between earthquakes, and the rate of this healing process plays a key role in determining earthquake stress drop[1–4], rupture characteristics[5,6] and seismic scaling relations[2–4,7]. Frictional healing (as evidenced by increasing static friction during quasi-stationary contact between two surfaces[1,8–12]) is considered the mechanism most likely to be responsible for fault strengthening[2,3,13,14]. Previous studies, however, have shown a large discrepancy between laboratory and seismic (field) estimates of the healing rate[2–4,14,15]; in the laboratory, rock friction changes by only a few per cent per order-of-magnitude change in slip rate, whereas seismic stress drop increases by a factor of 2 to 5 per order-of-magnitude increase in earthquake recurrence interval. But in such comparisons, it is assumed that healing and static friction are independent of loading rate. Here, I summarize laboratory measurements showing that static friction and healing vary with loading rate and time, as expected from friction theory[16–18]. Applying these results to seismic faulting and accounting for differences in laboratory, seismic and tectonic slip rates, I demonstrate that post-seismic healing is expected to be retarded for a period of several hundred days following an earthquake, in agreement with recent findings from repeating earthquakes[13,14,19,20].

The problem of how faults regain strength between earthquakes is crucial for our understanding of the seismic cycle and the physics of earthquake rupture. Several factors could play a role, such as interaction of geometric irregularities and fault-zone heterogeneity[7], but frictional strengthening is likely to be a key effect in any case. Seismic data indicate that earthquake stress drop increases logarithmically with time[2,3,14] and rock friction studies show that static friction (which would correspond to fault yield strength) increases with log(time) (refs 1, 9–12). Critical factors in understanding these observations are the connection between stress drop and fault strength, and the problem of scaling laboratory friction observations to earthquake faults. Previous studies have assumed that static friction data can be applied directly, whereas the results summarized here indicate that static friction and time-dependent strengthening are system responses, dependent on loading rate and elastic coupling.

Figure 1 shows friction data from experiments in which simulated fault gouge (breccia and wear material within fault zones) was sheared in a servocontrolled testing apparatus. Frictional healing $\Delta\mu$ is measured as the difference between static and initial friction; the data indicate that static friction and $\Delta\mu$ increase with hold time and loading rate (Fig. 1), consistent with previous work[1,8,9,18]. The experiments include instantaneous changes in loading rate (Fig. 1), which show that the effect of loading rate on static friction is significantly larger than on steady-state sliding friction. Temporal characteristics of the data and measurements of changes in relative porosity of the gouge $\Delta\phi$ indicate that shear strength decays logarithmically with time during healing and that gouge compacts with the same temporal form (Fig. 2), consistent with previous work[21,22]. The data indicate that static friction and healing rate ($\beta = \Delta\mu/\Delta\log_{10}t_h$, where t_h is hold time) vary systematically with loading rate over a range of t_h spanning three orders of magnitude (Fig. 1). In particular, a ten times increase in loading rate has about the same effect on $\Delta\mu$ as a ten times increase in hold time.

The data have three important implications. (1) They indicate that laboratory measurements of static friction and time-dependent healing must be scaled appropriately for comparison with seismic estimates of fault healing. Previous comparisons have assumed that fault healing can be derived directly from the steady-state velocity dependence of sliding friction[2–4,15]. (2) The observation that restrengthening is a system response, dependent on loading velocity, indicates that the rate of fault healing is expected to vary during the seismic cycle. (3) The observation that porosity decreases with

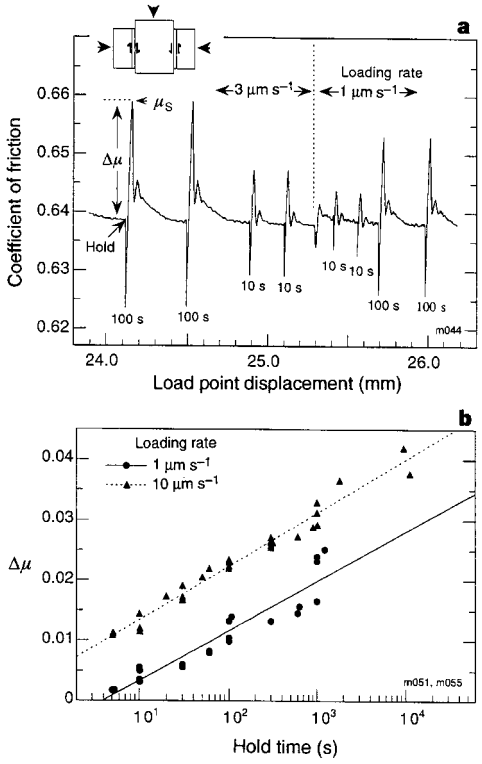

Figure 1 Friction data from experiments in which gouge layers were sheared within rough granite surfaces in the double-direct-shear configuration (upper inset). **a**, Plot of the coefficient of friction versus displacement of a control point where shear load is applied. Load point displacement is controlled with a high-speed, servo-hydraulic actuator. Data are shown for slide-hold-slide tests at loading rates of 1 and 3 μm s^{-1} and hold times of 10 and 100 s. The coefficient of static friction, μ_s, is the maximum value reached following a hold, and $\Delta\mu$ is the difference between static and sliding friction. Hold times given below data indicate positions at which loading was stopped and fault surfaces were held in quasi-stationary contact. Frictional strength relaxes during holds due to fault creep and finite apparatus stiffness. Inset shows double-direct-shear configuration. The testing apparatus consists of two independently servocontrolled load frames applying shear and normal forces across the sample. Stiffness of the vertical frame is 225 MPa cm^{-1} expressed as shear stress per load point displacement. Nominal frictional contact dimension is 10 cm × 10 cm and gouge layers are initially 2.1 mm thick. Initial gouge particle size is 50–150 μm and rock surface roughness (r.m.s.) ~200 μm. During shearing, normal stress is held constant at 25 MPa and changes in layer thickness are recorded continuously to ±0.1 μm. **b**, Frictional healing data for two loading rates as a function of hold time. The data indicate that $\Delta\mu$ and β are functions of hold time and loading rate, with higher loading rates yielding greater healing for a given time. Lines indicate best-fit log-linear relations. Healing rates $\beta = \Delta\mu/\Delta\log_{10}t_h$ are: 0.0082 for 1 μm s^{-1}, and 0.0086 for 10 μm s^{-1}.

log(hold time), coupled with the dependence of both $\Delta\phi$ and $\Delta\mu$ on loading rate, implies that porosity is closely related to the evolution of frictional strength as suggested in theoretical and experimental studies[21–23].

An important point is the origin of the loading-rate dependence of $\Delta\mu$ and β: why does static frictional strength vary with loading rate? The observation that healing varies approximately as the product of loading rate and hold time implies that the mechanism is a function of time and slip. As this is a property of rate- and state-dependent friction (RSF) laws, which are capable of modelling a wide range of seismic phenomena[4,18,24–27], I evaluate the present data in the context of these laws. In RSF relations[16,17] the coefficient of friction μ is written as:

$$\mu = \mu_0 + a \ln\left(\frac{V}{V_0}\right) + b \ln\left(\frac{V_0\theta}{D_c}\right) \quad (1)$$

$$\frac{d\theta}{dt} = 1 - \frac{V\theta}{D_c} \quad (2)$$

where μ_0 is a constant appropriate for steady-state slip at velocity V_0, V is the frictional slip rate, D_c is a critical slip distance, θ is a state variable, and a and b are empirical constants. Equation (2) describes the evolution of frictional state following a perturbation in velocity as proposed by Dieterich[16]. Other evolution laws have been proposed[6,17] but the distinction is not important here. To model laboratory friction data, equations (1) and (2) are coupled with a description of elastic interaction between the loading system and sliding surfaces:

$$d\mu/dt = k(V_l - V) \quad (3)$$

where k is stiffness divided by normal stress, and V_l is loading velocity. Equations (1)–(3) are solved numerically, taking $V_l = V_0$, to yield friction curves for comparison with data.

In Fig. 3a I show a best-fit RSF model to a step change in loading rate. The main features of the data are well fitted, and the best-fit constitutive parameters are consistent with previous studies[9,28–30]. These parameters were used to obtain predictions of static friction and healing as a function of hold time and velocity (Fig. 3b). The predicted curves match the data for each loading rate, which is remarkable given that both $\Delta\mu$ and β are fitted for a set of loading rates with no free parameters. RSF laws are apparently capable of describing frictional strengthening as observed in experiment, and thus may be used to scale the laboratory results to different loading velocities.

In experiments the initial slip velocity and the subsequent loading rate are equal and varied together, whereas on earthquake faults the initial slip velocity would correspond, crudely, to the coseismic slip rate V_{cs} and the rate of subsequent loading, V_L, to the background tectonic loading rate. To estimate the effect of slip rate on fault healing I performed numerical simulations using equations (1)–(3) (Fig. 4a). The simulations use laboratory values for the parameters a and b, a field-based estimate for D_c, and $k = G/(L\sigma)$, where G is shear modulus, L is earthquake rupture dimension, and σ is the fault-normal effective stress. A reference case, in which $V_{cs} = V_L = 1\,\mu m\,s^{-1}$, indicates log-linear healing, as expected (Fig. 4a). To compare other cases, I consider only the change in static friction by subtracting the steady-state velocity effect on friction, given by $b - a = \Delta\mu/\Delta\ln V$. This is reasonable if friction during seismic rupture is limited by dynamic factors and is independent of static failure strength; however, only the absolute values of $\Delta\mu$ are affected in any case, not its time dependence. For coseismic slip rates of 0.01–1 m s^{-1} and loading rates approximately equal to plate tectonic rates (30 mm yr^{-1} $\approx 3 \times 10^{-9}$ m s^{-1}) static friction shows an initial period of retarded healing and an increase in healing rate after a few hundred days (Fig. 4a). Although the length of the initial period of delayed healing varies somewhat with stiffness (and thus earthquake size), the form of the curve does not.

In the simulations I used $k = 1 \times 10^{-5}\,\mu m^{-1}$ (which corresponds to $L = 30$ m for $G = 30$ GPa and $\sigma = 100$ MPa) for comparison with data from a set of small repeating earthquakes (Fig. 3b). The earthquakes are magnitude 1.5 events that repeatedly ruptured a small patch (radius $\approx$ 30 m, depth 6–8 km) of the Calaveras fault in California, with a range of inter-event times spanning nearly three orders of magnitude[13,14]. The data indicate that seismic stress drop increases with recurrence interval, and that the healing rate increases at about 100–300 days, in agreement with the numerical simulation (Fig. 4). Moreover, a reduced healing rate during the period immediately following earthquakes of similar size can be inferred from repeating earthquakes with shorter recurrence interval (<10–100 days), which do not show variation in stress drop with recurrence interval[19,20].

In the numerical simulations, the change in healing rate is the result of slip during frictional relaxation. This slip is akin to earthquake afterslip, in which post-seismic fault slip accumulates at a rate that decays approximately exponentially following some

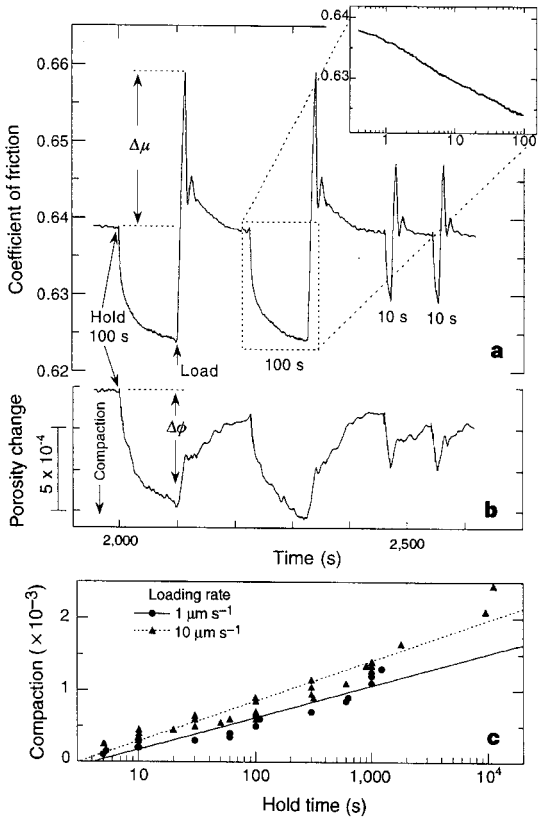

Figure 2 Experimental determination of variation of $\Delta\phi$ and $\Delta\mu$. **a** and **b**, plots of friction data (**a**) and relative porosity (**b**) versus time for the initial section of Fig. 1. Frictional strength decreases, and the gouge layers compact, during holds. The magnitude of $\Delta\phi$ and $\Delta\mu$ increase with hold time. Dilation of the gouge layers on reloading approximately equals time-dependent compaction, and thus porosity during steady-state shear is constant. Upper inset shows friction versus log(time) during hold and indicates that friction relaxes logarithmically with time. Porosity mimics friction variations during holds. Porosity data are obtained from measurements of layer thickness, using the nominal contact area to determine volume change, which is normalized by the initial gouge volume. A linear trend has been removed from the porosity data to account for geometric thinning of the gouge layer during shear. **c**, Compaction $\Delta\phi$ associated with healing is shown versus hold time for two loading rates. Like the frictional healing data, $\Delta\phi$ is a function of hold time and loading rate, with higher loading rates yielding greater healing for a given time. Lines indicate best-fit log-linear relations.

seismic events[24,31]. The RSF laws show (equation (2)) that afterslip would tend to erase the effects of frictional healing until slip velocity $V \ll D_c/\theta$. Thus for hold times that are short compared with the time necessary for afterslip to slow sufficiently—about 100 days in the simulations—frictional healing is partially erased (Fig. 4a). This same effect produces concave-up curvature in laboratory data for short hold times (shorter than those shown here; Fig. 1), which is consistent with the view that strengthening involves chemical cementation and contact junction growth, and is disrupted by slip.

The agreement between the simulations and the repeating-earthquake data implies that similar processes may operate in earthquake fault zones. But when considering the rough agreement between the long-term healing rates of Fig. 4 it must be noted that changes in static strength are a function of both β and effective normal stress. I have used laboratory β values reported here and a normal effective lithostatic gradient, which yields higher effective normal stress than some field estimates[4]. Lower normal stress would require higher frictional healing rates, which is consistent with enhancement of

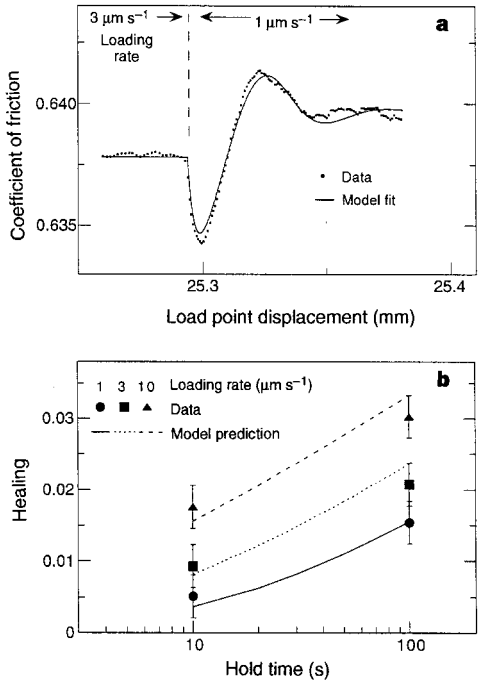

Figure 3 Use of an RSF model to analyse loading-rate dependence. **a**, Friction data for a step decrease in loading rate (as shown in Fig. 1a) together with a best-fit RSF model determined by iterative least-squares inversion of equations (1)–(3). The best-fit constitutive parameters (see text) are: $a = 0.0066$, $b = 0.0083$, $D_c = 7.1\,\mu$m. These data show velocity weakening frictional behaviour (the steady-state coefficient of sliding friction decreases with slip velocity). Complete stress–displacement curves for similar experiments[29] show that sliding friction evolves to a steady value over 3–6 mm of slip and undergoes a transition from velocity strengthening to velocity weakening at engineering shear strains of 4–5. The critical slip distance, D_c (a measure of the slip or shear strain needed to reach a new steady-state friction upon a perturbation in slip rate) also evolves over this interval[29]. **b**, Measurements of healing ($\Delta\mu$) for three loading rates, together with prediction of the rate and state friction law. Model predictions use the constitutive parameters determined in **a** and thus the dependence of $\Delta\mu$ and β on loading rate and hold time are fitted with no free parameters. Error bars show typical experimental reproducibility.

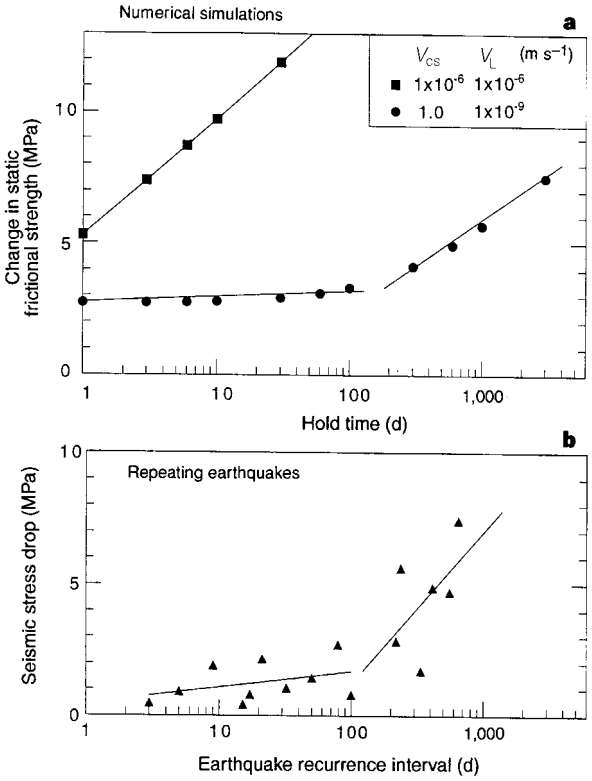

Figure 4 Results of numerical simulations and comparison with field data. **a**, Numerical simulations of fault healing in which initial slip velocity (corresponding to coseismic slip) V_{cs} and subsequent loading rate (corresponding to tectonic loading) V_L are varied. In this model, hold time corresponds to earthquake recurrence interval. Frictional strength is derived from static friction assuming an effective fault normal stress of 100 MPa. For $V_{cs} = V_L = 1\,\mu$m s^{-1}, static strength increases linearly with log(time). Taking V_{cs} as 1 m s^{-1} and V_L as 10^{-9} m s^{-1} (typical values for earthquake particle velocity and plate tectonic loading rates, respectively) indicates that the effective healing rate is retarded for the period immediately following an earthquake. The duration of reduced healing scales with fault stiffness and thus earthquake rupture dimension, which is taken as 30 m. Friction parameters are $a = 0.01$, $b = 0.02$, and $D_c = 5$ mm, consistent with laboratory and field estimates[29]. **b**, Seismic stress drop versus recurrence interval for a series of repeating earthquakes[13,14]. The data indicate a distinct break in slope, reflecting a lower healing rate for events with recurrence interval $<\approx 100$ days. In the numerical simulations shown in **a** such variations in healing rate are due to afterslip. In both panels lines indicate best-fit log-linear relations for times <100 days and >100 days.

healing by thermal and chemical effects[4,11,12]. But even for effective fault-normal stress as low as 10 MPa, the simulations of Fig. 4 do not indicate the apparent discrepancy between laboratory and seismic estimates of fault healing noted in earlier works[2–4,15]. This is because those works used an effective slip velocity, derived from D_c and the earthquake recurrence interval, which is not a correct approach[31]. Frictional healing rate β scales as $b\ln t_h$ for long hold times (from equations (1) and (2), $V \ll D_c/\theta$ as t_h becomes large, which yields $d\theta/dt \approx 1$ and thus $\Delta\mu(t_h)$ proportional to $b\ln t_h$), whereas the approach based on effective velocity assumes that healing and fault strength scale as $\Delta\mu(t_h) \approx (b - a)\ln t_h$. This indicates that the comparison of laboratory and field estimates of fault healing should involve absolute values rather than relative changes. Using this approach, I note that the average healing rate from repeating earthquakes[14] and seismic scaling relations[2–4] is ~3 MPa per decade and the long-term rate from repeating earthquakes (Fig. 4b) is ~6 MPa per decade. This compares with the long-term healing rate inferred from laboratory data of 4.5 MPa per decade (Fig. 4a), depending on b and effective normal stress, which is in much better agreement than previous comparisons. □

Received 29 May; accepted 21 October 1997.

1. Dieterich, J. H. Time-dependent friction in rocks. *J. Geophys. Res.* **77,** 3690–3697 (1972).
2. Scholz, C. H., Aviles, C. A. & Wesnousky, S. G. Scaling differences between large interplate and intraplate earthquakes. *Bull. Seismol. Soc. Am.* **76,** 65–70 (1986).
3. Kanamori, H. & Allen, C. R. in *Earthquake Source Mechanics* (eds Das, S., Boatwright, J. & Scholz, C.) 227–236 (Am. Geophys. Un., Washington DC, 1986).
4. Scholz, C. H. *The Mechanics of Earthquakes and Faulting* (Cambridge Univ. Press, New York, 1990).
5. Heaton, T. Evidence for and implications of self healing pulses of slip in earthquake rupture. *Phys. Earth Planet Inter.* **64,** 1–20 (1990).
6. Perrin, G., Rice, J. R. & Zheng, G. Self-healing slip pulse on a frictional surface. *J. Mech. Phys. Solids* **43,** 1461–1495 (1995).
7. Heimpel, M. Critical behaviour and the evolution of fault strength during earthquake cycles. *Nature* **388,** 856–858 (1997).
8. Johnson, T. Time dependent friction of granite: implications for precursory slip on faults. *J. Geophys. Res.* **86,** 6017–6028 (1981).
9. Beeler, N. M., Tullis, T. E. & Weeks, J. D. The roles of time and displacement in the evolution effect in rock friction. *Geophys. Res. Lett.* **21,** 1987–1990 (1994).
10. Nakatani, M. & Mochizuki, H. Effects of shear stress applied to surface in stationary contact on rock friction. *Geophys. Res. Lett.* **23,** 869–872 (1996).
11. Karner, S. L., Marone, C. & Evans, B. Laboratory study of fault healing and lithification in simulated fault gouge under hydrothermal conditions. *Tectonophysics* **277,** 41–55 (1997).
12. Olsen, M. P., Scholz, C. H. & Léger, A. Healing and sealing of a simulated fault gouge under hydrothermal condtions: implications for fault healing. *J. Geophys. Res.* (submitted).
13. Vidale, J. E., Ellsworth, W., Cole, A. & Marone, C. Rupture variation with recurrence interval in eighteen cycles of a small earthquake. *Nature* **368,** 624–626 (1994).
14. Marone, C., Vidale, J. E. & Ellsworth, W. Fault healing inferred from time dependent variations in source properties of repeating earthquakes. *Geophys. Res. Lett.* **22,** 3095–3098 (1995).
15. Cao, T. & Aki, K. Effect of slip rate on stress drop. *Pure Appl. Geophys.* **124,** 515–529 (1986).
16. Dieterich, J. H. Modeling of rock friction: 1. Experimental results and constitutive equations. *J. Geophys. Res.* **84,** 2161–2168 (1979).
17. Ruina, A. Slip instability and state variable friction laws. *J. Geophys. Res.* **88,** 10359–10370 (1983).
18. Kato, N., Yamamoto, K., Yamamoto, H. & Hirasawa, T. Strain-rate effects on frictional strength and the slip nucleation process. *Tectonophysics* **211,** 269–282 (1992).
19. Nadeau, R. M., Foxall, W. & McEvilly, T. V. Clustering and periodic recurrence of microearthquakes on the San Andreas fault at Parkfield, California. *Science* **267,** 503–508 (1995).
20. Lees, J. M. Microseismic multiplets do not exhibit effects of fault healing at Coso. *Eos* **77,** 502 (1996).
21. Wang, W. & Scholz, C. H. Micromechanics of the velocity and normal stress dependence of rock friction. *Pure Appl. Geophys.* **143,** 303–316 (1994).
22. Beeler, N. M. & Tullis, T. E. The roles of time and displacement in velocity dependent volumetric strain of fault zones. *J. Geophys. Res.* **102,** 22595–22609 (1997).
23. Segall, P. & Rice, J. R. Dilatancy, compaction, and slip instability of a fluid infiltrated fault. *J. Geophys. Res.* **100,** 22155–22173 (1995).
24. Marone, C., Scholz, C. H. & Bilham, R. On the mechanics of earthquake afterslip. *J. Geophys. Res.* **96,** 8441–8452 (1991).
25. Rice, J. R. Spatio-temporal complexity of slip on a fault. *J. Geophys. Res.* **98,** 9885–9907 (1993).
26. Dieterich, J. H. A constitutive law for rate of earthquake production and its application to earthquake clustering. *J. Geophys. Res.* **99,** 2601–2618 (1994).
27. Roy, M. & Marone, C. Earthquake nucleation on models faults with rate and state dependent friction: the effects of inertia. *J. Geophys. Res.* **101,** 13919–13932 (1996).
28. Biegel, R. L., Sammis, C. G. & Dieterich, J. H. The frictional properties of a simulated gouge with a fractal particle distribution. *J. Struct. Geol.* **11,** 827–846 (1989).
29. Marone, C. & Kilgore, B. Scaling of the critical slip distance for seismic faulting with shear strain in fault zones. *Nature* **362,** 618–621 (1993).
30. Beeler, N. M., Tullis, T. E., Blanpied, M. L. & Weeks, J. D. Frictional behaviour of large displacement experimental faults. *J. Geophys. Res.* **101,** 8697–8716 (1996).
31. Marone, C. Laboratory-derived friction laws and their application to seismic faulting. *Annu. Rev. Earth Planet. Sci.* (in the press).

Acknowledgements. I thank C. Scholz and N. Beeler for review comments and J. Rice, M. Blanpied and C. Raymo for discussions that helped sharpen my understanding of frictional healing. This work was supported by the US NSF.

Correspondence should be addressed to the author (e-mail: cjm@westerly.mit.edu).

Biodiversity inventories, indicator taxa and effects of habitat modification in tropical forest

J. H. Lawton*, D. E. Bignell†#, B. Bolton‡, G. F. Bloemers*‡#, P. Eggleton‡, P. M. Hammond‡, M. Hodda‡#, R. D. Holt§, T. B. Larsen‖, N. A. Mawdsley*‡#, N. E. Stork‡#, D. S. Srivastava*# & A. D. Watt¶

* *NERC Centre for Population Biology, Imperial College, Silwood Park, Ascot SL5 7PY, UK*
† *School of Biological Sciences, Queen Mary and Westfield College, University of London, London E1 4NS, UK*
‡ *The Natural History Museum, Cromwell Road, London SW7 5BD, UK*
§ *Museum of Natural History, University of Kansas, Lawrence, Kansas 66045, USA*
‖ *358 Coldharbour Lane, London, SW9 8LP, UK*
¶ *Institute of Terrestrial Ecology, Bush Estate, Penicuick, Midlothian, EH26 0QB, UK*

Despite concern about the effects of tropical forest disturbance and clearance on biodiversity[1,2], data on impacts, particularly on invertebrates, remain scarce[3–8]. Here we report a taxonomically diverse inventory on the impacts of tropical forest modification at one locality. We examined a gradient from near-primary, through old-growth secondary and plantation forests to complete clearance, for eight animal groups (birds, butterflies, flying beetles, canopy beetles, canopy ants, leaf-litter ants, termites and soil nematodes) in the Mbalmayo Forest Reserve, south-central Cameroon. Although species richness generally declined with increasing disturbance, no one group serves as a good indicator taxon[9–12] for changes in the species richness of other groups. Species replacement from site to site (turnover) along the gradient also differs between taxonomic groups. The proportion of 'morphospecies' that cannot be assigned to named species and the number of 'scientist-hours' required to process samples both increase dramatically for smaller-bodied taxa. Data from these eight groups indicate the huge scale of the biological effort required to provide inventories of tropical diversity, and to measure the impacts of tropical forest modification and clearance.

We chose birds and butterflies as groups to study because they frequently serve as 'flagship taxa' in biodiversity inventories[6,9,13]. The other six groups were chosen because they are all widespread and abundant invertebrates. The study area[14–16] is semi-deciduous humid forest representative of much of southern Cameroon, and is used for subsistence farming, experimental agriculture, and forestry trials[16], providing a mosaic of habitats. Study sites (Table 1) formed a gradient of increasing intensity and frequency of disturbance. For some taxa the inventories are almost complete; for others, because of lower sampling effort, they are far from complete (Table 2). The proportion of 'morphospecies'[11] (judged by expert systematists) that cannot currently be assigned to known (named) species is inversely related to log (body length) ($F_{1,5} = 11.07$, $P = 0.02$, ants included only once; values $>x$ in Table 2 regressed as x), emphasizing the huge disparity that exists between groups in the state of taxonomic knowledge.

Generally, as in previous studies[1,2,5–7,17,18], species richness

Present addresses: TBCU, University of Malaysia Sabah, 88999 Kota Kinabalu Sabah, Malaysia (D.E.B); Central Science Laboratory, Plant Health Group, Sand Hutton, York YO4 1LZ, UK (G.F.B.); Australian National Insect Collection, CSIRO Division of Entomology, GPO Box 1700, Canberra, Australia (M.H.); Department of Biology, University of Leeds, Leeds, LS2 9JT, UK (N.A.M.); Cooperative Research Centre for Tropical Rainforest Ecology and Management, PO Box 6811, Cairns, Queensland 4870, Australia (N.E.S.); and Centre for Biodiversity Research, Faculty of Science, University of British Columbia, Vancouver, British Columbia V6T 1Z4, Canada (D.S.S.)